Hindawi Publishing Corporation
Advances in Condensed Matter Physics
Volume 2010, Article ID 258019, 6 pages
doi:10.1155/2010/258019

Research Article

Infrared Optical Response of Metallic Graphene Nanoribbons

Zigang Duan,[1] Wenhu Liao,[2] and Guanghui Zhou[2]

[1] *Key Laboratory of Optoelectronic Devices and Systems of Ministry of Education and Guangdong Province, Shenzhen University, Shenzhen 518060, China*
[2] *Department of Physics and Key Laboratory for Low-Dimensional Structures and Quantum Manipulation (Ministry of Education), Hunan Normal University, Changsha 410081, China*

Correspondence should be addressed to Guanghui Zhou, ghzhou@hunnu.edu.cn

Received 22 December 2009; Revised 25 April 2010; Accepted 25 April 2010

Academic Editor: Yuri Galperin

We investigate theoretically the infrared optical response characteristics of metallic armchair/zigzag-edge graphene nanoribbons (A/ZGNRs) to an external longitudinally polarized electromagnetic field at low temperatures. Within the framework of linear response theory at the perturbation regime, we examine the optical infrared absorption threshold energy, absorption power, dielectric function, and electron energy loss spectra near the neutrality points of the systems. It is demonstrated that, by some numerical examples, the photon-assisted direct interband absorptions for AGNR exist with different selection rules from those for ZGNR and single-walled carbon nanotube at infrared regime. This infrared optical property dependence of GNRs on field frequency may be used to design graphene-based nanoscale optoelectronic devices for the detection of infrared electromagnetic irradiations.

1. Introduction

Intriguing experimental [1] and theoretical [2–11] attentions have been paid to graphene-based electronics, especially the unique electronic [3–11] and transport properties [12–19] of GNRs due to its potential applications in nanodevices. The optical spectra [20] of semiconducting GNRs and the excitonic effects [21, 22] in the optical properties of AGNRs with many-electron effects included have been investigated by density functional theory and the first-principles calculations, respectively. Liu et al. [23] have demonstrated that magnetic field can enhance and tune the optical response of GNRs in the terahertz to far-infrared regime. The effects of intrinsic spin-orbit and Coulomb interactions on low-energy properties of AGNRs have been studied [24]. The optical absorption selection rule [25] for ZGNR has been proposed to be qualitatively different from that for armchair carbon nonotubes (CNTs) [26, 27]. The optical properties of AGNRs [28] irradiated under an longitudinal polarized electromagnetic field have also been analyzed. Zhang et al. [29] have investigated the magneto-optical properties of graphene quantum dots. Furthermore, the optical response of the ZGNRs with the spin interaction included has been found to be dominated by magnetic edge-state-derived excitons other than the affections of the edges and confinement on the optical transition energies. [30, 31] However, to the best of our acknowledge, the optical properties for driven GNRs [20–25, 28–31] in the important frequency band of infrared have seldom been involved.

A N-AGNR is either semiconducting or metallic depending on the number of dimer lines N along the edge. However, an N-ZGNR is always metallic due to its edge states. In this paper, we present a theoretical investigation on the infrared properties in the vicinity of neutrality points for the two types of metallic GNRs under the irradiation of an external longitudinal polarized low-frequency field at low temperatures. The dependence of the optical absorption threshold values, absorption power, dielectric function, and electron energy loss spectrum (EELS) on the irradiation energy are demonstrated in the framework of linear response theory under the dipole approximation [25, 28, 29]. Some new interband absorptions are predicted with the exception of the quantitative description of threshold energy on the width of GNRs, and the results are discussed and compared with those in the previous works [20–31].

The rest of the paper is organized as follows. The analytical expressions of the band spectra close to the neutrality points for A/ZGNRs, the optical absorption power, dielectric function, and electron energy loss spectra are calculated in Section 2. Some numerical examples and discussions for the results are demonstrated in Section 3. Finally, Section 4 concludes the paper.

2. Model and Formulism

The tight-binding π electron dispersion relation for an ideal infinite graphene sheet can be solved exactly as [3, 4, 10, 11]

$$\epsilon_{k_x,k_y} = \pm\gamma\left[3+2\cos\left(k_y a\right)\pm 4\left|\cos\left(\frac{k_y a}{2}\right)\cos\left(\frac{\sqrt{3}k_x a}{2}\right)\right|\right]^{1/2}, \tag{1}$$

where the hopping integral $\gamma = 2.75\,\text{eV}$, the minimal translation distance of honeycomb lattice is $a = 2.46\,\text{Å}$, and the variation range of k_x and k_y should be specified for particular GNRs.

Employing the hard-wall boundary conditions to longitudinal wave function for a N-AGNR, that is, $\phi_{A/B}(0) = \phi_{A/B}(N+1)=0$, one gets the discretized wave vector $k_y = m\pi/[(N+1)a]$, and further obtains the rationalized band spectrum in terms of continuous k_x (longitudinal) and discrete m (transversal) quantum numbers near the point of neutrality [10, 11]

$$\epsilon_{n,k_x} = \pm\gamma\left[3+2\cos\frac{(j^*+n)\pi}{N+1}-4\cos\frac{(j^*+n)\pi}{2(N+1)}\cos\frac{\sqrt{3}k_x a}{2}\right]^{1/2}, \tag{2}$$

where $\pm$ represents, respectively, the conduction bands (CB) and valence bands (VB), $j^*=2(N+1)/3$ is the lowest/highest CB/VB mode with $n = 0, 1, 2,\ldots, N-j^*$, and the longitudinal wave vector is confined within the first Brillouin zone $0\leq|\sqrt{3}k_x a|\leq\pi$.

Distinct from AGNR, the discrete values of k_y for an N-ZGNR are k_x-dependent, [10, 11] which is determined by

$$\frac{\sin(\kappa_n N)}{\sin\left[\kappa_n(N+1/2)\right]} = \pm 2\cos\left(\frac{k_x a}{2}\right), \tag{3}$$

where $\kappa_n=\sqrt{3}k_y a$. Therefore, one obtains $\epsilon_{n,k_x} = \pm\gamma\sin(\kappa_n/2)/\sin\left[\kappa_n(N+1/2)\right]$ by substituting (3) into (1) and the real solutions $\kappa_n = (n+1/2)\pi/N$ of the extrema for the conduction bands by equation $\sin(\kappa_n N)/\sin\left[\kappa_n(N+1)\right] = N/(N+1)$, where $n = 0,1,2,\ldots,n \ll N$. Therefore, the band spectrum for a N-ZGNR can be induced as [10, 11]

$$\epsilon_{n,k_x} = \pm\gamma\left[\frac{3}{4}\left(k_x a-\frac{2\pi}{3}\right)^2+\frac{(n+1/2)^2\pi^2}{4N^2}\left(1+\frac{\sqrt{3}\pi}{3}-\frac{\sqrt{3}k_x a}{2}\right)\right]^{1/2}, \tag{4}$$

with the exception of the edge states and the continuous variable k_x is restricted to the range of $0 \leq |k_x a| \leq \pi$. However, when k_x falls into the interval $2\pi/3 < |k_x a| \leq \pi$, the imaginary solution of (3) reads

$$\epsilon_{0,k_x} = \pm\gamma\frac{\sinh[-\ln[2\cos(k_x a/2)]]}{\sinh[-(2N+1)\ln[2\cos(k_x a/2)]]}, \tag{5}$$

which gives the edge states (make ZGNRs always metallic) localized on the edge and decay exponentially into the center. The $\pm$ in (4) and (5) represents the CB and VB, respectively.

Using the perturbation theorem in the dipole-transition approximation, the optical absorption power for perfect GNRs irradiated under a longitudinally polarized weak electromagnetic field can be expressed as

$$P(\omega) = \frac{4\pi e^2 E_0^2}{m_e^2\omega}\sum_{n_1,n_2,k_x}\left[f(\epsilon_{n_1,k_x})-f(\epsilon_{n_2,k_x})\right] \times |\langle n_1,k_x|\hat{p}_x|n_2,k_x\rangle|^2\delta(\epsilon_{n_2,k_x}-\epsilon_{n_1,k_x}-\hbar\omega), \tag{6}$$

where E_0 and ω are the intensity and frequency of the irradiation field, respectively, m_e is the free-electron mass, $f(\epsilon_{n,k_x})$ the Fermi-Dirac distribution function, and $n_{1/2}$ the subband indices for the VB/CB, while $\hat{p}_x$ is the x-component of the momentum operator. Furthermore, the imaginary part of the complex dielectric function $\xi_2(\omega)$ can be obtained as

$$\xi_2(\omega) = \frac{8\pi^2 e^2}{m_e^2\omega^2}\sum_{n_1,n_2,k_x}\left[f(\epsilon_{n_1,k_x})-f(\epsilon_{n_2,k_x})\right] \times |\langle n_1,k_x|\hat{p}_x|n_2,k_x\rangle|^2\delta(\epsilon_{n_2,k_x}-\epsilon_{n_1,k_x}-\hbar\omega), \tag{7}$$

and one gets the real part of the dielectric function $\xi_1(\omega)$ by Kramers-Kronig transformation [26–28]

$$\xi_1(\omega) = 1+\frac{4}{\pi}\wp\int_0^\infty\frac{\omega'\xi_2(\omega')}{\omega'^2-\omega^2}d\omega', \tag{8}$$

where $\wp$ denotes the integral principal value. Therefore, at the long-wavelength limit [26–28], one can obtain EELS by $-\Im m\,[\xi(\omega)^{-1}]$ while $\Im m$ represents the imaginary part, the refractive index, and reflectivity from the complex dielectric function ξ for the systems.

3. Results and Discussions

In the following, we present the numerical examples of the calculated P, ξ_2, and EELS for two types of GNRs under the irradiation of a longitudinal polarized electromagnetic field. In the calculation, the Dirac delta function in (6) and (7) is simulated [26–28] as $\delta(x) = e^{-x^2\Gamma^{-2}}/(\Gamma\pi^{1/2})$ with the Gaussian broadening factor $\Gamma = 0.014\,\text{eV}$. The coupling between the sp^2 states and the p_z state is neglected since we are only interested in the optical response of the GNRs near the zero-energy points, that is, at the low energy regime [29]. Under the irradiation of a weak electromagnetic

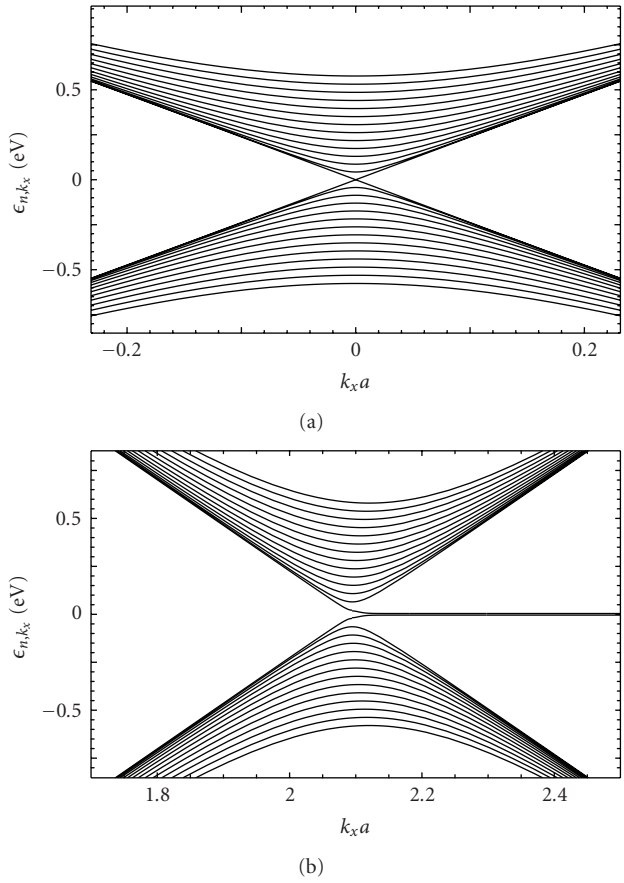

Figure 1: Electron band structures for perfect (a) 173-AGNR and (b) 100-ZGNR. The lattice constant along the nanoribbons is $a = 2.46\,\text{Å}$.

field, the dipole transition matrix elements $\langle n_1, k_x|\hat{p}_x|n_2, k_x\rangle$ within the tight-binding single-electron picture [25, 28] are chosen as 0.206. Since the wavelength (several hundreds of nanometer) of the weak infrared field is much larger than the transversal size (about 42.5 nanometer) of the 173-AGNR and 100-ZGNR, one can ignore the local-field correction in the present systems. [21, 22, 26, 27] Furthermore, the excitonic effects can also be ignored since the electron-electron interaction has not been included in this work [21, 22, 26, 27].

In Figure 1, we present the electronic structures ϵ_{n,k_x} versus the longitudinal wave vector k_x near the neutrality points of 173-AGNR and 100-ZGNR in panel (a) and (b), respectively. As is seen the 173-AGNR case from Figure 1(a), the CB, and the VB are mirror symmetric with respect to the Fermi level $E_F = 0$, and the CB subbands at $k_x = 0$ correspond (from bottom to top in sequential order) to $n = 0,1,2,\ldots,13$. Moreover, Figure 1(b) the 100-ZGNR case presents an armchair-CNT-like [25] electron band structure other than the lowest/highest conduction/valence band, which converts from an almost linear decrease/increase for $k_x a \leq 2.09$ to an exponential-like (governed by (5)) curve up to the edge of the first Brillouin zone, while the sequence for the other subbands of the CB is $n = 1,2,\ldots,13$ from

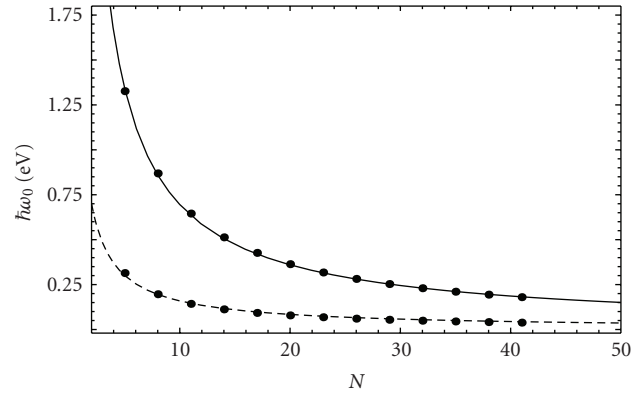

Figure 2: Threshold energy for GNRs as a function of their width. The solid line fits for AGNRs and the dashed line for ZGNRs.

bottom to top. When the electromagnetic field is polarized longitudinally, the allowed optical absorptions for CNTs [26, 27] are restricted to vertical excitations (i.e., n and k_x remain unchanged) between the VB and the CB, while those for ZGNRs [25] are from V_0 (V_{odd}) to C_{odd} (C_0) in the low energy range, where V_0 and C_0 denote the highest valence and the lowest conduction subband, respectively, while the oddth and eventh conduction and valence subbands for GNRs are denoted as C/V_{odd} and C/V_{even}. As follows, different optical absorptions will be demonstrated from the calculated $P(\omega)$ and $\xi_2(\omega)$ at vanishing $\partial\epsilon_{n,k_x}/\partial k_x$ for longitudinally irradiated A/ZGNRs.

The threshold energy $\hbar\omega_0$ (the optical transition energy between the highest valence subband and the second conduction subband or that from the second highest valence subband to the lowest conduction one for AGNR, while it is the optical transition from/to the edge states for ZGNR) as a function of the GNRs width is shown in Figure 2. As expected, the wider the ribbons, the lower the threshold energy (decreasing from visible to infrared). It is observed that the discretized points can be fitted by $6.20 \times N^{-0.95}$ and $1.32 \times N^{-0.92}$ for AGNRs (see the solid line in Figure 2) and ZGNRs (the dashed line in Figure 2), respectively, therefore, the threshold energy for AGNRs is more sensitive to width than that for ZGNRs since the electronic properties of AGNRs are more sensitive to their geometries [20, 21].

The optical absorption power P (in arbitrary units) near the neutrality points of 173-AGNR and 100-ZGNR as a function of the irradiation energy is demonstrated in Figure 3. In the presence of an external irradiation field, a peak in $P(\omega)$ indicates a direct absorption photon with energy $\hbar\omega$ followed by a transition from the VB to the CB. As illustrated in Figure 3(a) for the 173-AGNR case, the absorption peaks at 0.041, 0.129, 0.217, 0.305, 0.393, 0.484, and 0.575 eV can be identified to the transitions $V_0(V_i) \rightarrow C_i(C_0)$, as denoted by p_{0i} with $i = 1,3,\ldots,13$ in Figure 3(a), while those at 0.085, 0.173, 0.261, 0.349, 0.44, and 0.531 eV result from the excitations $V_0(V_j) \rightarrow C_j(C_0)$ as denoted by p_{0j} with $j = 2,4,\ldots,12$ in Figure 3(a), respectively. It is worthwhile to note that some vertical transitions (with unchanged k_x and subband indices) have been shown.

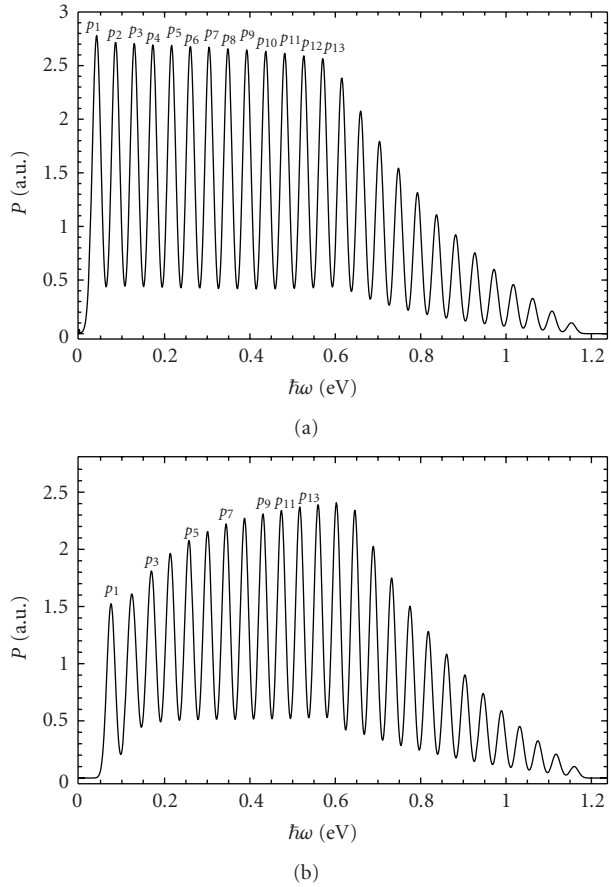

Figure 3: Optical absorption power for (a) 173-AGNR and (b) 100-ZGNR as a function of the irradiation energy.

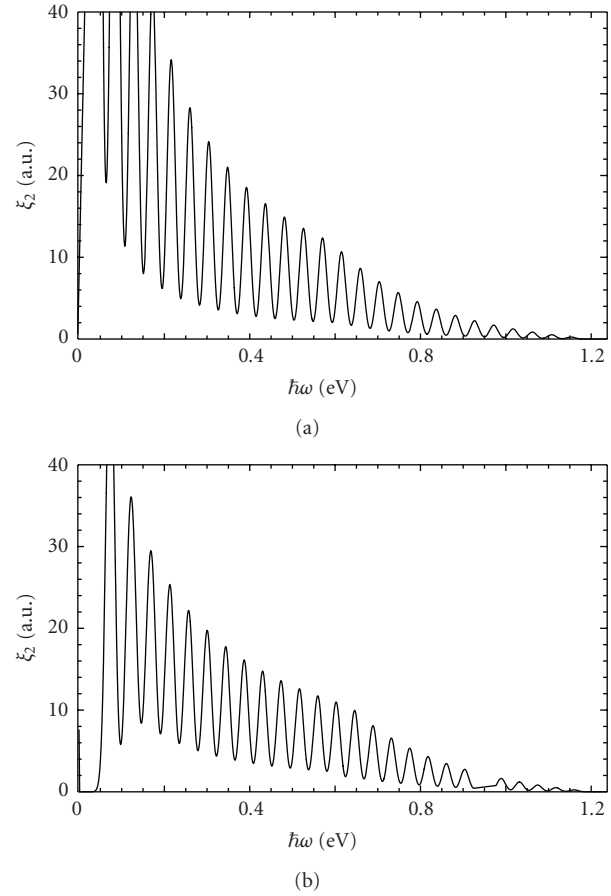

Figure 4: Imaginary part of the dielectric function for (a) 173-AGNR and (b) 100-ZGNR as a function of photon energy.

For example, the peaks at 0.616, 0.792, 0.974, and 1.152 eV should rely on the excitations from $V_7 \rightarrow C_7$, $V_9 \rightarrow C_9$, $V_{11} \rightarrow C_{11}$, and $V_{13} \rightarrow C_{13}$, while the absorptions at 0.704, 0.88, and 1.062 eV may be from $V_8 \rightarrow C_8$, $V_{10} \rightarrow C_{10}$, and $V_{12} \rightarrow C_{12}$, respectively. However, one can owe the peaks at 0.66, 0.748, 0.836, 0.924, 1.015, and 1.108 eV to the transitions from V_{odd} (V_{even}) to C_{even} (C_{odd}) similarly as [28]. Furthermore, Figure 3(b) exhibits the 100-ZGNR case. One can identify those absorption peaks at 0.074, 0.168, 0.25, 0.347, 0.429, 0.486, and 0.512 eV to the transitions between the decaying modes (edge states) and the odd*th* subbands, as denoted by p_{0i} with $i = 1,3,\ldots,13$ in Figure 3(b), respectively. The resonance structures at 0.072, 0.215, 0.303, 0.388, 0.476, 0.561, 0.646, 0.732, 0.817, 0.902, 0.99, and 1.075 eV may be attributed to the vertical transitions between the VB and the CB. It should be pointed out that the current results are different from the absorption coefficient of the monolayer graphene [32] in the optical range of frequencies due to the quantum confinement and different optical transitions. It is noted that the optical absorptions for AGNR are stronger than those for ZGNR at the regime of $0 < \hbar\omega < 0.66$ eV and decrease slower in the higher energy range.

Furthermore, the imaginary part of the dielectric function ξ_2 (in arbitrary units) as a function of photon energy is illustrated in Figure 4. As shown in Figure 4(a) for the 173-ANGR case, one notes a series of resonance structures, corresponding to the absorption peaks in Figure 3(a), which are much higher in the low energy range since $\xi_2 \propto P/\omega$. In correspondence to the optical transitions in Figure 3(b), the 100-ZGNR case (see Figure 4(b)) presents a set of relative lower resonance peaks, especially at the low energy regime. It seems that AGNR is more sensitive to the low frequency infrared than ZGNR, which is consistent with [23, 28]. One notices that the imaginary dielectric function ξ_2 for both 173-AGNR and 100-ZGNR demonstrates several zero points (corresponding to plasma frequencies of the systems) at the higher energy regime.

The EELS of the two systems as a function of the irradiation field energy is demonstrated finally in Figure 5. Since the system EELS is combined with the complex dielectric function ξ simply by $-\Im m\,[\xi^{-1}]$ (see [26–28]), Figure 5(a) (the 173-AGNR case) shows a set of singular peaks at 0.55, 0.688, 0.77, 0.825, 0.853, 0.88, 0.935, 0.963, 0.99, 1.018, 1.045, and 1.155 eV corresponding to the plasmon frequencies (zero points of ξ_1, not shown here) while the 100-ZGNR case (see Figure 5(b)) presents some sharp peaks at 0.765, 0.798, 0.847, 0.963, 0.99, and 1.073 eV with much lower ones at 0.935, 1.018, and 1.155 eV than the 173-AGNR

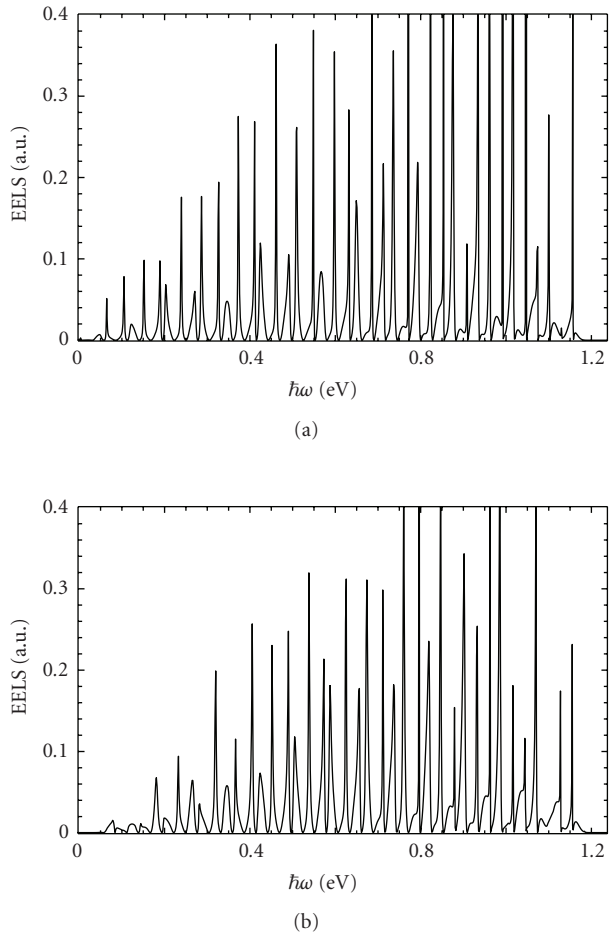

Figure 5: EELS for (a) 173-AGNR and (b) 100-ZGNR as a function of the irradiation energy.

case. It seems that there are more plasmon modes for AGNR than for ZGNR in the infrared range, while the fine details [26, 27] of the system EELS may be smoothed out by a larger broadening parameter.

4. Conclusion

In summary, using the linear response theory, we have investigated theoretically the optical properties of semi-infinite clean A/ZGNR under the irradiation of an external longitudinal polarized low-frequency electromagnetic field at low temperatures. Under the dipole-transition approximation, it is shown that the optical absorption power, dielectric function and electron energy loss spectrum of the systems are sensitive to the infrared irradiation depending on the chirality and the width of GNRs. Some new photon-assisted direct interband transitions are proposed. The predicted optical properties are expected to be observed by scanning tunneling microscopy optical spectroscopy [33, 34] and reflection contrast spectroscopy [35] experiments and used to design the graphene-based nanoscale optoelectronic devices [36–38].

Acknowledgments

This work was supported by the National Natural Science Foundation of China (Grant no. 10974052), Specialized Research Fund for the Doctoral Program of Higher Education of China (Grant no. 20060542002).

References

[1] Y.-M. Lin, V. Perebeinos, Z. Chen, and P. Avouris, "Electrical observation of subband formation in graphene nanoribbons," *Physical Review B*, vol. 78, no. 16, Article ID 161409, 2008.

[2] Y.-W. Son, M. L. Cohen, and S. G. Louie, "Half-metallic graphene nanoribbons," *Nature*, vol. 444, no. 7117, pp. 347–349, 2006.

[3] L. Brey and H. A. Fertig, "Electronic states of graphene nanoribbons studied with the Dirac equation," *Physical Review B*, vol. 73, no. 23, Article ID 235411, 2006.

[4] L. Yang, C.-H. Park, Y.-W. Son, M. L. Cohen, and S. G. Louie, "Quasiparticle energies and band gaps in graphene nanoribbons," *Physical Review Letters*, vol. 99, no. 18, Article ID 186801, 2007.

[5] Y.-W. Son, M. L. Cohen, and S. G. Louie, "Energy gaps in graphene nanoribbons," *Physical Review Letters*, vol. 97, no. 21, Article ID 216803, 2006.

[6] D. Gunlycke and C. T. White, "Tight-binding energy dispersions of armchair-edge graphene nanostrips," *Physical Review B*, vol. 77, no. 11, Article ID 115116, 2008.

[7] M. Y. Han, B. Özyilmaz, Y. Zhang, and P. Kim, "Energy band-gap engineering of graphene nanoribbons," *Physical Review Letters*, vol. 98, no. 20, Article ID 206805, 2007.

[8] K. Nakada, M. Fujita, G. Dresselhaus, and M. S. Dresselhaus, "Edge state in graphene ribbons: nanometer size effect and edge shape dependence," *Physical Review B*, vol. 54, no. 24, pp. 17954–17961, 1996.

[9] S. Okada, "Energetics of nanoscale graphene ribbons: edge geometries and electronic structures," *Physical Review B* , vol. 77, no. 4, Article ID 041408, 2008.

[10] L. Malysheva and A. Onipko, "Spectrum of π Electrons in graphene as a macromolecule," *Physical Review Letters*, vol. 100, no. 18, Article ID 186806, 2008.

[11] L. I. Malysheva and A. I. Onipko, "Quantum conductance of achiral graphene ribbons and carbon tubes," *Journal of Experimental and Theoretical Physics*, vol. 108, no. 1, pp. 126–131, 2009.

[12] Y. P. Chen, Y. E. Xie, and X. H. Yan, "Electron transport of L-shaped graphene nanoribbons," *Journal of Applied Physics*, vol. 103, no. 6, Article ID 063711, 2008.

[13] H. Xu, T. Heinzel, M. Evaldsson, and I. V. Zozoulenko, "Magnetic barriers in graphene nanoribbons: theoretical study of transport properties," *Physical Review B*, vol. 77, no. 24, Article ID 245401, 2008.

[14] F. Zhai and K. Chang, "Theory of huge tunneling magnetoresistance in graphene," *Physical Review B*, vol. 77, no. 11, Article ID 113409, 2008.

[15] L. Brey and H. A. Fertig, "Elementary electronic excitations in graphene nanoribbons," *Physical Review B*, vol. 75, no. 12, Article ID 125434, 2007.

[16] Q. Liang, Y. Yu, Q. Wang, and J. Dong, "Controllable 0-π transition in a superconducting graphene-nanoribbon junction," *Physical Review Letters*, vol. 101, no. 18, Article ID 187002, 2008.